iScience

Article

Patient-derived rhabdomyosarcoma cells recapitulate the genetic and transcriptomic landscapes of primary tumors

Generation of RMS Patient-Derived Cell Models

Head and Neck

Extremities

Urogenital Tract

Extremities

RMS Patient

Tumor Tissue

RNA Sequencing

RMS PDC

Genetic Profile

In Vitro Culture

Hallmark Gene Validation

Application

RMS PDC

Drug Screening

Genetic Profile

Gene

Drug

Correlation Analysis

Yuxiang Hu, Ziqi He, Shuangai Liu, ..., Meidan Ying, Jinhu Wang, Ting Tao

mying@zju.edu.cn (M.Y.)
wjh@zju.edu.cn (J.W.)
taot@zju.edu.cn (T.T.)

Highlights

Generation of 9 patient-derived cells (PDCs) for rhabdomyosarcoma (RMS)

RMS PDCs maintain the expression of RMS hallmark genes in matched tissues

RMS PDCs retain the genetic alterations of matched tissues

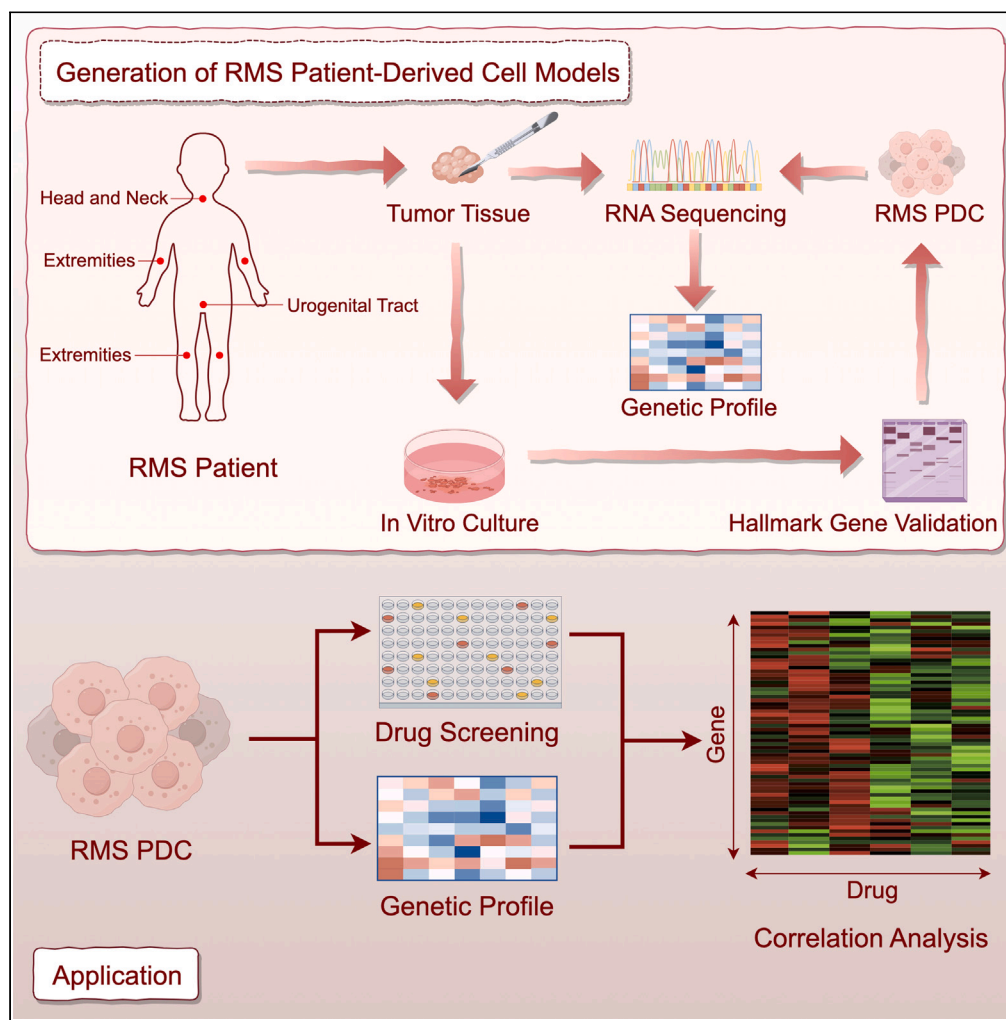RMS PDCs provide valuable tools to assess pharmacogenomic interactions

Article

Patient-derived rhabdomyosarcoma cells recapitulate the genetic and transcriptomic landscapes of primary tumors

Yuxiang Hu,[1,2,3,8] Ziqi He,[1,2,3,8] Shuangai Liu,[1,2,3] Wenwen Ying,[4] Yifan Chen,[4] Manli Zhao,[5] Min He,[1,2] Xuan Wu,[1,2] Yinbing Tang,[1,2] Weizhong Gu,[5] Meidan Ying,[1,4,7,*] Jinhu Wang,[1,2,6,7,*] and Ting Tao[1,2,6,7,9,*]

SUMMARY

Rhabdomyosarcoma (RMS) is the most common soft tissue sarcoma in childhood and adolescence. The availability of appropriate and well-characterized preclinical models for RMS is limited, posing a challenge for investigating the molecular mechanisms and evaluating new targeted compounds in preclinical settings. Here, we collected 51 RMS specimens (referred to as ZJUCH-RMS cohort) and established 9 patient-derived cells (PDCs) and validated the identity of these cells by the expression of RMS-specific markers. Whole-transcriptome analysis identified high-confidence mutations in ZJUCH-RMS cohort including *RAS*, *TP53*, *ARID1A*, *MYOD1*, and *MYCN*. Further studies showed that RMS PDCs retained the genetic alterations and the expression of RMS hallmark and dependency genes in matched primary tumors and acted as valuable tools to assess drug responses and pharmacogenomic interactions. Our study provides unique PDCs that are available for preclinical studies of RMS and further advances the feasibility of RMS PDCs as valuable tools for developing personalized treatments for patients.

INTRODUCTION

Rhabdomyosarcoma (RMS) is the most common soft tissue sarcoma in childhood and adolescence, which accounts for about 7% of solid tumors and 50% of soft tissue sarcomas in children.[1] The annual incidence of RMS in children under 20 years of age is ∼4.5 patients per million, with a slight male predominance (male/female = 1.37:1).[1,2] This malignancy represents a high-grade neoplasm composed of skeletal myoblast-like cells, demonstrating notable local invasiveness and a robust tendency to metastasize.[3,4] By combining morphologic features and molecular genetics, the 2020 World Health Organization (WHO) classification divides RMS into four subtypes: embryonal (ERMS), alveolar (ARMS), spindle/sclerosing cell (SRMS), and pleomorphic (PRMS).[5] Despite advances in multimodal therapy, including surgery, chemotherapy, and radiation therapy, the prognosis for RMS remains guarded, particularly in cases of metastatic or recurrent disease.[6] The five-year overall survival rate is 70–90% for ERMS and 50–70% for ARMS.[3,7] Understanding the molecular mechanisms underlying RMS pathogenesis and progression is crucial for developing targeted therapies and improving outcomes for affected patients. Further, preclinical models serve as essential tools for evaluating the efficacy and safety of potential therapeutics. However, the availability of appropriate and well-characterized preclinical models for RMS is limited, posing a challenge for investigating the molecular mechanisms and evaluating new targeted compounds in preclinical settings.

Over the past few decades, cancer cell lines have played crucial roles in cancer research, serving as invaluable tools for studying various aspects of cancer biology, including tumor initiation, progression, and drug response. Two large-scale dataset of cultured cancer cells and their pharmacology have been described and provided valuable information for personalized therapeutic regimens.[8,9] Cell lines also offer a convenient platform for conducting mechanism studies and target verifications in biomedical studies, benefiting from the availability of numerous tools. For RMS, 18 ERMS and 12 ARMS cell lines have been reported to be used in various studies from the literature.[10] However, the long-term culture of cell lines may produce potential pitfalls during cancer research. First, these cell lines may acquire additional mutations, which make them no longer accurately replicate the characteristics of the original tumor. Second, there may be nomenclature errors and

[1]Pediatric Cancer Research Center, National Clinical Research Center for Child Health, Hangzhou 310052, China
[2]Department of Surgical Oncology, Children's Hospital Zhejiang University School of Medicine, National Clinical Research Center for Child Health, Hangzhou 310052, China
[3]The First Clinical Institute, Zunyi Medical University, Zunyi 563000, China
[4]Institute of Pharmacology and Toxicology, Zhejiang Province Key Laboratory of Anti-Cancer Drug Research, College of Pharmaceutical Sciences, Zhejiang University, Hangzhou 310058, China
[5]Department of Pathology, Children's Hospital Zhejiang University School of Medicine, National Clinical Research Center for Child Health, Hangzhou 310052, China
[6]Key Laboratory of Diagnosis and Treatment of Neonatal Diseases of Zhejiang Province, Hangzhou 310052, China
[7]Cancer Center, Zhejiang University, Hangzhou 310058, China
[8]These authors contributed equally
[9]Lead contact
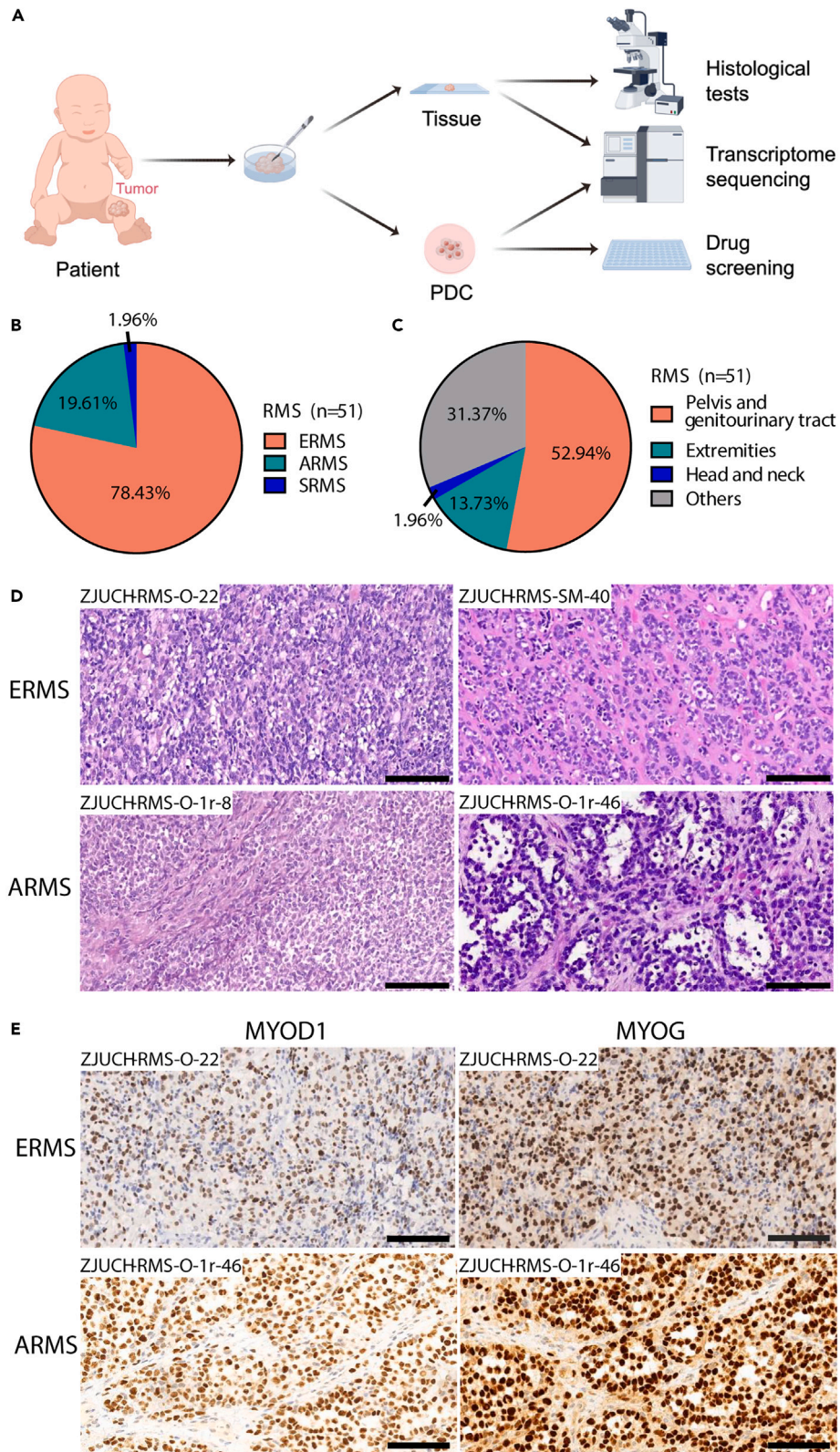*Correspondence: mying@zju.edu.cn (M.Y.), wjh@zju.edu.cn (J.W.), taot@zju.edu.cn (T.T.)
https://doi.org/10.1016/j.isci.2024.110862

A

Patient → Tissue → Histological tests

PDC → Transcriptome sequencing

Drug screening

B

1.96%

19.61%

78.43%

RMS (n=51)
ERMS
ARMS
SRMS

C

31.37%

52.94%

1.96%

13.73%

RMS (n=51)
Pelvis and genitourinary tract
Extremities
Head and neck
Others

D

ERMS

ZJUCH-RMS-O-22

ZJUCH-RMS-SM-40

ARMS

ZJUCH-RMS-O-1r-8

ZJUCH-RMS-O-1r-46

E

MYOD1

MYOG

ERMS

ZJUCH-RMS-O-22

ZJUCH-RMS-O-22

ARMS

ZJUCH-RMS-O-1r-46

ZJUCH-RMS-O-1r-46

Figure 1. Characterization of rhabdomyosarcoma patient samples in ZJUCH-RMS cohort
(A) Schematic diagram for the RMS samples processing and establishment of RMS PDCs. This figure is created with Figdraw.
(B and C) Pie charts showing the subtypes (B) and tumor locations (C) of RMS in ZJUCH-RMS cohort.
(D) Histological features of two main subtypes of RMS (ERMS and ARMS) were observed under hematoxylin and eosin (H&E) staining. Scale bars, 100 μm.
(E) Representative images of two main subtypes of RMS (ERMS and ARMS) by immunohistochemical staining for MYOD1 and MYOG. Scale bars, 100 μm.

cross-contamination between cell lines. The misidentification of cell lines currently is estimated to be between 15% and 35%, highlighting the significant challenges in ensuring the accuracy of cellular research and data interpretation.[10,11]

In the ongoing process of research, a number of new cancer cell lines have been established and subjected to various characterizations and applications. For example, Lee et al. established large-scale of patient-derived cells (PDCs) across 14 different tumor types and demonstrated clinical consistency between drug sensitivity and clinical response based on these PDCs, emphasizing the prospect of personalized treatment guided by drug screening.[11] Qiu et al. generated 50 PDCs from hepatocellular carcinoma patients and established a pharmacogenomic landscape in liver cancers, providing a useful resource for drug discovery.[12,13] Both studies demonstrated genetic and transcriptomic similarity between PDCs and primary tumors, highlighting their potential as representative models for studying tumor biology and therapeutic responses.

In this study, we collected 51 RMS specimens (referred to as ZJUCH-RMS cohort) and established 9 PDCs from these samples, and validated the identity of these cells by the expression of RMS-specific markers. RNA sequencing (RNA-seq) was performed to profile the genetic alterations in ZJUCH-RMS cohort and to compare the transcriptome and genetic mutations between the PDCs and matched primary tumors. The ZJUCH-RMS cohort exhibited mutations in various genes including *RAS* family genes, *TP53*, *ARID1A*, *MYOD1*, and *MYCN*. Further analysis showed that RMS PDCs retained the genetic alterations and the expression of RMS hallmark and dependency genes in matched primary tumors and acted as valuable tools to assess drug responses and pharmacogenomic interactions. Our study provides unique PDCs that available for preclinical studies of RMS and further advances the feasibility of RMS PDCs as valuable tools for developing personalized treatments for patients.

RESULTS

Generation and characterization of nine RMS PDCs from ZJUCH-RMS cohort

To generate and characterize RMS PDCs, we collected 51 RMS specimens (referred to as ZJUCH-RMS cohort) from Department of Surgical Oncology, Children's Hospital Zhejiang University School of Medicine and subjected to PDC culture (see STAR Methods for detail) and transcriptome sequencing (Figure 1A). The demographic characteristics of these samples were summarized in Tables S1 and S2. Most of the cases (n = 40, 78.43%) were diagnosed as ERMS, with 10 ARMSs (all *PAX3-FOXO1* fusion-positive by fluorescence *in situ* hybridization) and 1 SRMS (Figure 1B). They typical arose from immature skeletal myoblasts located at pelvis, genitourinary tract, and extremities (Figure 1C). ERMS presents as a mixed type of round and spindle-shaped cells, accompanied by myxoid stromal changes. The histology of ERMS resembles a combination of striated muscle cells at different stages of embryonal development: from small, round, undifferentiated cells, to tadpole-like cells, ribbon-shaped striated cells, and finally to fully differentiated rhabdomyoblasts (Figure 1D, top panel). The characteristics of ARMS include large nuclei, with abundant acidophilic cytoplasm and multinucleated tumor giant cells. Tumor cells aggregate at the edges of fibrous septa, resulting in alveolus-like structures (Figure 1D, bottom panel). All the tested specimens were immunohistochemical-positive for MYOD1 and MYOG (Figure 1E; Table S1), two skeletal muscle-specific nuclear regulatory proteins,[5] verifying the reliability of these samples in this cohort.

Nine RMS PDCs were established at 2–3 weeks from the 51 RMS specimens, including 7 ERMSs, 1 ARMS, and 1 SRMS (Figures 2A and S1; Table 1), with an overall success rate of 17.65%. Interestingly, the success rate was 17.5% for ERMS, and 10% for ARMS, though ARMS behaves more aggressively than ERMS clinically. Two of the PDCs were established from a single individual, with one pre-chemotherapy (ZJUCH-RMS-PDC-39BC) and the other post-chemotherapy (ZJUCH-RMS-PDC-39AC), providing ideal models to study the effects of chemotherapy on tumor biology and therapeutic responses. Morphologically, these PDCs typically displayed elongated or spindle-shaped cells with variable degrees of differentiation (Figure 2A). All the RMS PDCs could be cultured *in vitro* for more than 15 passages, with cell doubling time around 3–4 days (Figure 2B). Reverse transcription polymerase chain reaction (RT-PCR) of RMS hallmark genes showed that all the RMS PDCs expressed *MYOD1* and *DES*, and majority of them expressed *MYOG* and *MYF5* (Figure 2C). Interestingly, the post-chemotherapy PDC ZJUCH-RMS-PDC-39AC showed lower expression of *MYOG* and *DES*, as compared with the pre-chemotherapy one. These results indicated a possible cell lineage shift toward muscle stem-like cells upon chemotherapy, as reported by previous studies with single-cell RNA-seq.[14–16] Moreover, the ARMS PDC ZJUCH-RMS-PDC-15 maintained the *PAX3–FOXO1* fusion as detected by RT-PCR (Figure 2D). Immunofluorescence staining showed that these PDCs were positive for MYOD1 and MYOG, confirming the origin of skeletal muscle lineage (Figure 2E).

RMS PDCs retain the expression of RMS hallmark and dependency genes in primary tumors

To characterize the RMS PDCs and primary tumors at the transcriptional level, we performed RNA sequencing (RNA-seq) analysis for all the PDCs and primary tumors, as well as RMS cell lines PLA-802, RD and RH30. Six non-RMS, fibroblast-like PDCs derived from RMS tissues were also subjected to the same analysis. These non-RMS PDCs were characterized by the negative expression of *MYOD1* and *MYOG*. PDCs with less than 10 passages were used for the experiments. We also obtained the transcriptome data of 17 RMS cell lines and 3 fibroblast cell lines (RMS stroma origin) from Cancer Cell Line Encyclopedia (CCLE).[8] Pearson correlation based on the expression of RMS hallmark genes revealed that our RMS PDCs were closely correlated with existing RMS cell lines, and our non-RMS PDCs were closely correlated with the
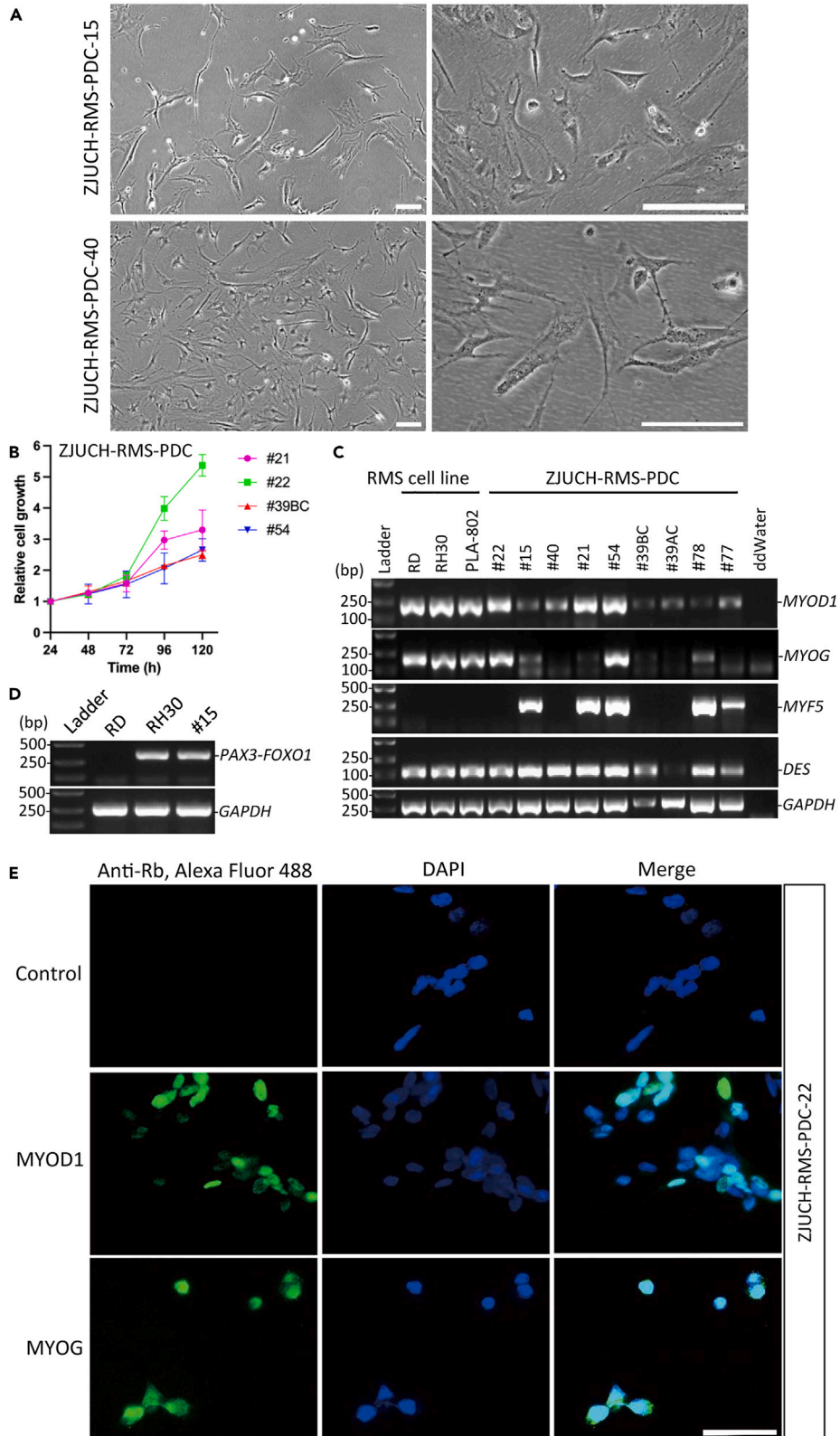
Figure 2. Establishment and characterization of nine rhabdomyosarcoma patient-derived cells

(A) Morphologies of two representative RMS PDCs including ZJUCH-RMS-PDC-15 and ZJUCH-RMS-PDC-40. Scale bars, 100 μm.

(B) Relative cell growth of RMS PDCs. Values represent means ± SEM of triplicate experiments. h, hours.

(C) Validation of RMS PDCs by RT-PCR for *MYOD1*, *MYOG*, *MYF5*, and *DES*. RMS cell lines RD, RH30, and PLA-802 were used as positive controls, double distilled water (ddWater) was used as negative control. GAPDH was used as a reference gene.

(D) Detection of *PAX3-FOXO1* fusion in ZJUCH-RMS-PDC-15 by RT-PCR. RMS cell line RD was used as negative control and RH30 as positive control. GAPDH was used as a reference gene.

(E) Immunofluorescence staining of a representative RMS PDC for MYOD1 and MYOG. Nuclei were stained with DAPI (blue). A staining without the primary antibody was used as control. Scale bar, 25 μm.

fibroblast cell lines (Figure 3A), demonstrating the robustness and fidelity of our PDC models in recapitulating the molecular characteristics of their respective counterparts. RMS hallmark genes including *MYOD1*, *MYOG*, *IGF2*, *FGFR4*, *ALK*, *DES*, *PAX3*, *PAX7*, *MYF5*, *MYF6*, and *MYCN*[17–19] were highly expressed in RMS PDCs and cell lines, while showing lowly or absent expression in non-RMS, fibroblast-like PDCs and fibroblast cells (Figure 3B).

To further explore the similarities and differences between RMS PDCs and matched primary tumors, we examined the expression of 386 RMS dependency genes (Table S3, based on cancer dependency map[20]). We found the expression of these dependency genes were well maintained in RMS PDCs compared to the corresponding tumor tissues, as well as RMS cell lines (Figure 3C). Principal component analysis (PCA) using this gene set showed that RMS PDCs, but not cell lines, clustered well with tumor tissues they are derived from (Figure 3D). Gene set enrichment analysis (GSEA) based on the whole transcriptome data revealed a main difference between RMS PDCs and tissues. Specifically, PDCs exhibited a loss of expression in genes enriched in myeloid and lymphoid cell lineages (Figures S2A and S2B), reflecting the absence of a tumor immune environment in the PDCs. Taken together, these data demonstrate RMS PDCs retain the major molecular features of tumor cells, albeit with apparent alterations in the immune landscape compared to tissues.

Genetic alterations identified in RMS of the ZJUCH-RMS cohort

We next sought to investigate the RMS PDCs and primary tumors in terms of genetic mutations. By analyzing the RNA-seq data from 51 primary tumors, we first identified 120 high-confidence variants involving 93 genes in the ZJUCH-RMS cohort, with a median of 3 high-confidence mutations in each of the 51 RMS samples (Figure S3; Table S4). The most frequently mutated high-confidence genes included *TP53* ($n = 10$, 19.61%), *NRAS* ($n = 9$, 17.65%), *ARID1A* ($n = 7$, 13.73%), and *HRAS* ($n = 6$, 11.76%) in this cohort (Figures 4A and S3). Mutations of *RAS* family genes (*NRAS*, *HRAS*, and *KRAS*) was exclusively identified in *PAX3-FOXO1* fusion-negative (PFN) ERMS cases (16 out of 40), resulting in a significant higher mutational frequency of *RAS* in PFN ERMS than in *PAX3-FOXO1* fusion-positive (PFP) ARMS ($p < 0.05$, two-tailed Fisher's exact test) (Figures 4A and 4B; Table S4). In addition, mutations of transcriptional factors *TP53*, *MYOD1* (L122R), and *MYCN* (P44T), as well as an epigenetic regulator *ARID1A*, were well identified in this cohort (Figure 4A; Table S4). *TP53*, a well-known tumor suppressor, was mutated in 9 out of 40 PFN ERMS cases, while only in 1 out of 10 PFP ARMS cases. Most of the *TP53* mutations occurred at DNA-binding domain, indicating a potential loss of DNA-binding ability of TP53 and suggesting a compromised tumor-suppressive function in these cases. Moreover, 60% of the RMS cases with *TP53* mutations exhibited anaplastic histology, which was significantly higher than that in *TP53*-wild-type group ($p < 0.001$, two-tailed Fisher's exact test) (Figure 4C). *MYOD1* and *MYCN* are both basic-helix-loop-helix (bHLH) transcriptional factors that play important roles in regulating cellular processes such as muscle differentiation, cell cycle progression, and oncogenesis. Previous studies have shown that *MYCN* is mutated at the same site (P44) in childhood neuroblastoma[21] and Wilms tumors,[22] suggesting a potential role for *MYCN* mutations in tumorigenesis across multiple pediatric cancers. Mutations in the chromatin remodeler *ARID1A* offer a potential therapeutic target for RMS, as ARID1B has been identified as a specific vulnerability in *ARID1A*-mutant cells in other tumors, including neuroblastoma and ovarian cancers.[23,24]

Table 1. The characteristics of RMS PDCs generated from ZJUCH-RMS cohort

| PDC	Gender	Age of diagnosis in years	Tumor location	Source (primary/metastasis/relapse)	Subtype	Time to establish (weeks)
ZJUCH-RMS-PDC-15	Female	16.39	Extremities	Primary	ARMS	2–3
ZJUCH-RMS-PDC-21	Female	1.33	Genitourinary	Primary	ERMS	2–3
ZJUCH-RMS-PDC-22	Female	0.73	Genitourinary	Primary	ERMS	2–3
ZJUCH-RMS-PDC-39BC	Male	4.30	Extremities	Primary	ERMS	2–3
ZJUCH-RMS-PDC-39AC	Male	4.30	Extremities	Primary	ERMS	2–3
ZJUCH-RMS-PDC-40	Male	5.41	Head and neck	Metastasis	ERMS	2–3
ZJUCH-RMS-PDC-54	Female	0.95	Genitourinary	Primary	ERMS	2–3
ZJUCH-RMS-PDC-77	Male	11.45	Trunk	Relapse	SRMS	2–3
ZJUCH-RMS-PDC-78	Male	0.85	Extremities	Primary	ERMS	2–3
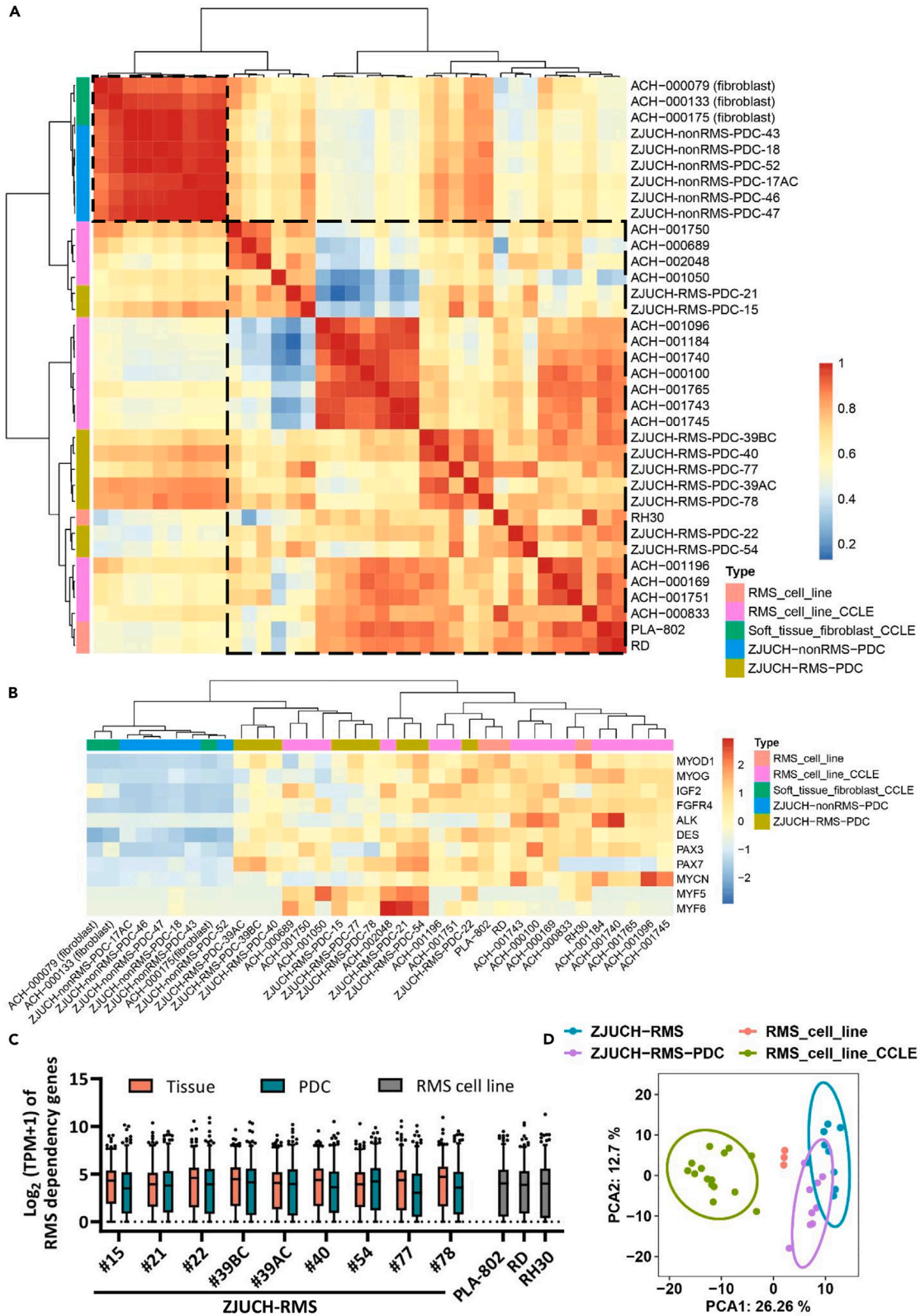
Figure 3. RMS PDCs retain the expression of RMS hallmark and dependency genes in primary tumors

(A) A heatmap of Pearson's correlation analysis based on $\log_2$ (TPM+1) of RMS hallmark genes from RNA-seq visualizing the correlation coefficients (r) between samples.

(B) Hierarchical clustering of the RMS hallmark genes based on $\log_2$ (TPM+1). Scale bar represents range of the relative expression levels.

(C) $\log_2$ (TPM+1) expression of RMS dependency genes (n = 386) in RMS PDCs and matched primary tumors. RMS cell lines were used as positive controls. Boxes indicate the median (horizontal line), 25th percentile and 75th percentile; Whiskers, 2.5–97.5th percentiles.

(D) PCA analysis of RMS cell lines, PDCs and matched primary tumors based on the expression of RMS dependency genes. A 95% confidence ellipse was shown for each group.

We then grouped theses high-confidence genes by their biological processes, and the top five most frequently mutated pathways were the MAPK signaling (n = 17, 33.33%), genome integrity (n = 13, 25.49%), chromatin SWI/SNF complex (n = 7, 13.73%), transcription factor (n = 6, 11.76%), and receptor tyrosine kinase (RTK) signaling (n = 4, 7.84%), all of which play crucial roles in regulating tumorigenesis (Figure 4D). Notably, the RAS-MAPK signaling pathway was most commonly altered in RMS, along with the activating mutations in *RAS* family members, including *NRAS* (G12S, G13D, and Q61 H/K/R), *HRAS* (G13 R/V and Q61 K/L), and *KRAS* (G12A), leading to constitutive activation of downstream signaling cascades. The pairwise associations of these high-confidence mutations were investigated, identifying a total of 20 pairs of significantly co-occurring genes ($p < 0.05$, two-tailed Fisher's exact test) (Figure 4E). Through this analysis, we detected several notable mutational associations in RMS. For instance, mutations in *MYCN*, *RAS*, *TP53*, and *MYOD1* frequently co-occur with other mutations. Significant interactions ($p < 0.05$, two-tailed Fisher's exact test) included *MYCN* with *ATM*, *CHEK2*, or *FRMPD1*; *NRAS* with *NCF1* or *COL2A1*; *HRAS* with *AIP*; *KRAS* with *PLCG1*; *TP53* with *MUTYH*, *CIC*, or *AIP*; and *MYOD1* with *NRAS* or *COL2A1*.

RMS PDCs retain the genetic alterations in matched primary tumors

To investigate whether the RMS PDCs retained the genetic mutations of their corresponding tumor tissues, we performed RNA-seq for all the nine RMS PDCs and compared the data with matched primary tumors. The majority of the high-confidence mutations were well preserved in PDCs as in matched tissues, including *MYOD1*, *NRAS*, *HRAS*, *ARID1A*, and *TP53* (Figure 5A; Table S5). The variant allele frequency (VAF) for each variant was comparable between each pair of samples (Figure 5B). Among these variants, *MYOD1* L122R, which harbors mutation in the bHLH domain, is the most prevalent one (Figure 5C). It has been reported that *MYOD1* with L122R mutation imparts a new c-MYC-site binding capability, possibly leading to a shift from cell differentiation to proliferation.[25,26] Further studies were needed to clarify the function of this variant in pathogenesis of RMS. Some RMS PDCs also gained a few additional mutations that were absent in the matched primary tumors, including mutations in *JMJD1C*, *NUP214*, *RUNX1*, *RELN*, *TRRAP*, and *CENPF*, with an average of less than 1 variant per sample (Figure 5A). Gene ontology (GO) analysis of these genes did not reveal any significantly enriched biological process or molecular function pathway, indicating the randomness of these mutations. Thus, RMS PDCs highly resemble the genetic features of their match primary tumors, demonstrating the fidelity and reliability of the PDC models in preclinical studies.

Effects of chemotherapeutic agents on RMS PDCs

To test the feasibility of RMS PDCs as valuable tools for evaluating drug responses, we performed drug screening using a library of 278 compounds, including targeted anti-cancer drugs and chemotherapeutic agents (Figure S4A; Table S6). The efficacy of these compounds varied among different RMS PDCs, with a cluster of several chemotherapeutic agents and targeted anti-cancer drugs involved in DNA damage and repair, epigenetics, and protein tyrosine kinase inhibition showing broad efficacy across all PDCs (Figure S4B). The relationship between gene mutation and drug sensitivity was predicted by oncoPredict, for example, mutations in *RUNX1* conferred resistance to compounds rubitecan and CB-5083, while enhancing sensitivity to other compounds (Figure S4C; Table S7).

We next focused on the efficacy of common chemotherapeutic agents on RMS PDCs. All the PDCs showed a higher sensitivity to actinomycin D (IC_{50}: 1.50–7.89 nM), doxorubicin (IC_{50}: 76.68–1392.00 nM), epirubicin (IC_{50}: 63.97–1661.00 nM), pirarubicin (IC_{50}: 25.2–1637.00 nM), and topotecan (IC_{50}: 33.85–1004.00 nM), while a lower sensitivity to etoposide (IC_{50}: 8511.00–91092954.00 nM) (Figures 6A and S5). We further found that three PDCs (refer to as AL-VCR-VDS-res group) showed more chemoresistance than the other six (refer to as AL-VCR-VDS-sen group) for anlotinib, vincristine, and vindesine (Figure 6B). By integrated analysis with the gene mutations data, we were intriguingly to find that all the PDCs in the AL-VCR-VDS-res group harbored RAS-activating mutations, while no such mutations were found in the PDCs of the AL-VCR-VDS-sen group ($p < 0.05$, two-tailed Fisher's exact test) (Figure 6C). Analysis of the transcriptome data between these two groups showed that RAS signaling pathway was activated in the AL-VCR-VDS-res group (Figure 6D), which is consistent with the activating mutations of *RAS* family genes. The activation of RAS pathway may cf. chemoresistance of RMS PDCs for anlotinib, vincristine, and vindesine, as previous studies in osteosarcoma and B cell precursor acute lymphoblastic leukemia showed similar results.[27,28] Anlotinib is a small molecule inhibitor targeting multiple RTKs, thereby affecting the RTK-RAS-MAPK signaling cascade within cells,[29] activation of RAS may lead to anlotinib resistance by circumventing the inhibitory effects of the drug on RTK signaling. Moreover, GSEA analysis showed significantly enriched pathways involved in spindle organization and assembly in the AL-VCR-VDS-res group (Figure 6E). As vincristine and vindesine work by interfering with microtubule formation and disrupting the mitotic spindle apparatus during cell division, the upregulation of these pathways suggests potential mechanisms of resistance to vincristine and vindesine in this group. Taken together, our results demonstrated the viability of RMS PDCs as valuable tools to assess drug responses, as well as the gene-drug associations, which will provide insights into clinical practices and potentially guide personalized treatment strategies.
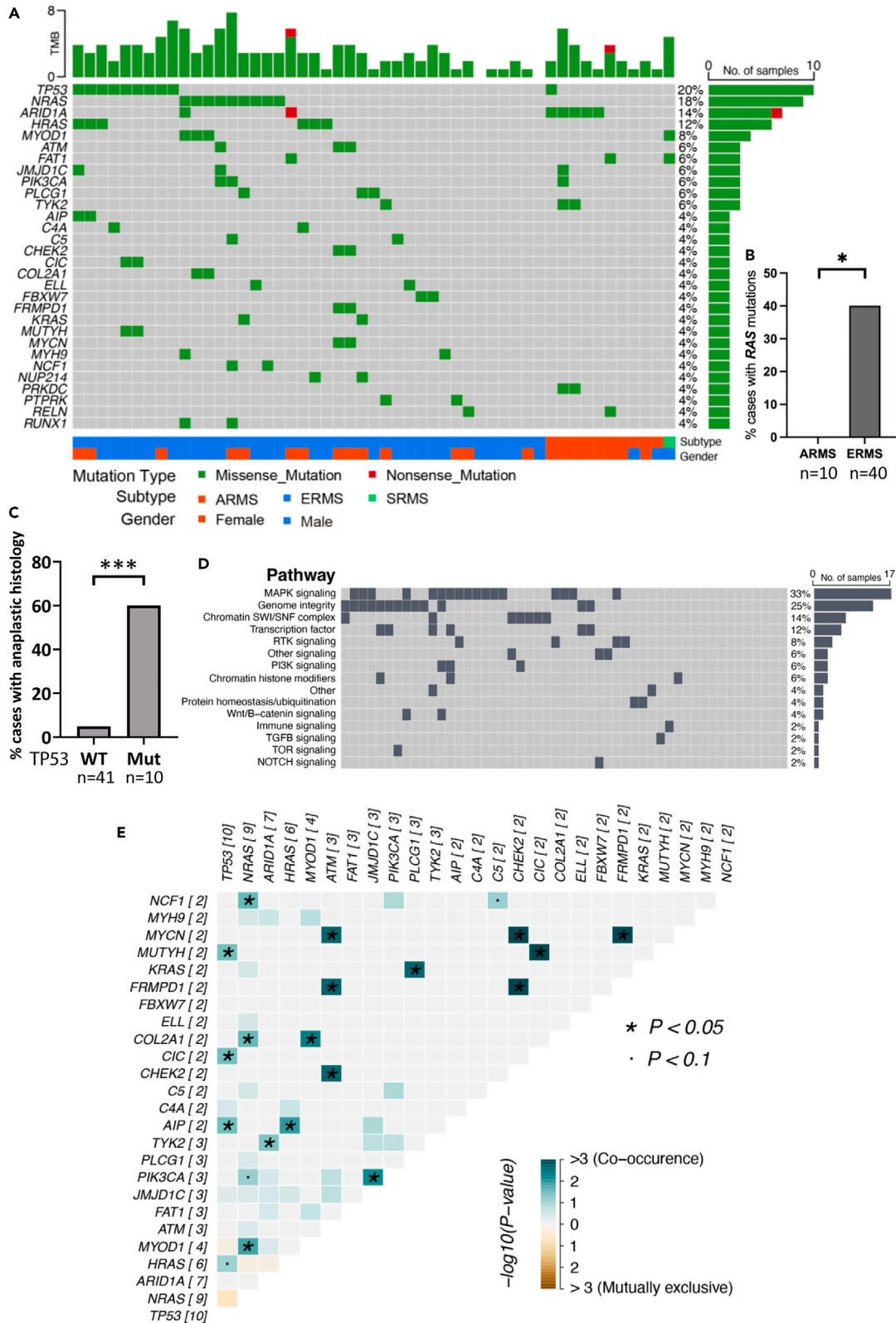
Figure 4. Genetic alterations of RMS identified in the ZJUCH-RMS cohort

(A) An oncoplot displaying top 30 genes with high-confidence mutations identified from RNA-seq analysis in 51 RMS samples. Genes are ordered by their mutation frequencies, with the tumor mutation burden (TMB) for each sample shown at the top of the panel, the number and percentage of samples for each gene shown at the right of the panel, and RMS patients information at the bottom of the panel.

(B) Frequencies of mutations in *RAS* family genes (*NRAS*, *HRAS*, and *KRAS*) in ARMS and ERMS were compared using the two-tailed Fisher's exact test. *$p < 0.05$.

(C) Percentages of RMS cases with anaplastic histology in *TP53*-wildtype (WT) and mutant (Mut) groups were compared using the two-tailed Fisher's exact test. ***$p < 0.001$.

(D) Top 15 biological pathways ordered by their mutation frequencies. The number and percentage of samples for each pathway are shown at the right of the panel.

(E) A heatmap displaying pairwise co-occurrence (in blue) and mutual exclusivity (in yellow) correlations between high-confidence genes. The statistical analysis was performed by two-tailed Fisher's exact test.

DISCUSSION

Preclinical models are invaluable tools in biomedical research, providing insights into disease mechanisms, facilitating drug discovery and development, and paving the way for personalized medicine approaches. However, the availability of appropriate and well-characterized pre-clinical models for RMS is limited. Here, we established 9 RMS PDCs from primary tumors, and showed that RMS PDCs retained the genetic alterations and the expression of RMS hallmark and dependency genes in matched primary tumors. RMS PDCs act as valuable tools to study RMS biology, drug responses, and pharmacogenomic interactions, which advances the feasibility of these PDCs for developing personalized treatments for patients. Although cell lines offer a consistent and reproducible experimental system for biological studies, they may accumulate genetic alterations over time in culture, diverging from the original tumors.[10] In contrast, PDCs maintain genetic stability closer to the original tumor, offering a more reliable model for evaluating drug responses. Previous studies have established patient-derived xenograft (PDX) and organoid models for RMS, providing an essential support for basic and translational research for this disease.[30–33] These models can be typically identified in 4–8 weeks, with feasibility of personalized drug screening. On the other hand, PDCs take much shorter time to establish, and exhibit a relatively higher successful rate, as compared to PDXs.[11] Drug screening with PDCs can be conducted on a large scale, in a patient-specific manner, and within a short time frame, which may benefit patients with personalized therapies.

Previous studies have shown that RAS pathway is mutationally activated in approximately 45% of PFN RMS cases,[34,35] which are similar to our results. The RAS-MAPK signaling pathway plays a critical role in the pathogenesis of RMS.[36] Dysregulation of this pathway is commonly observed in RMS, leading to uncontrolled cell proliferation, survival, and differentiation. Activating mutations in *RAS* family members are frequently detected in RMS. Additionally, aberrant activation of RTKs, such as FGFR4 and IGF1R, can drive RAS-MAPK pathway activation in RMS.[29] It has been reported that mutations or activation of RAS pathway can lead to resistance to multiple drugs. For examples, anlotinib resistance in osteosarcoma is mediated by the VEGFR/RAS/CDK2 pathway,[27] and RAS pathway-mutated cells are more resistant to vincristine in pediatric B cell precursor acute lymphoblastic leukemia.[28] Our data showed that three RMS PDCs with RAS-activating mutations exhibited increased resistance for anlotinib, vincristine, and vindesine than the other six, demonstrating the potential roles of RAS pathway dysregulation in chemotherapy resistance in rhabdomyosarcoma. Targeted inhibition of the RAS-MAPK pathway components represents a promising therapeutic strategy for RMS, aiming to impede tumor growth and improve patient outcomes.

TP53 germline mutations are reported to be associated with nonalveolar, anaplastic histology in 11 RMS cases.[37] Here, we showed that *TP53* mutations were enriched in PFN ERMS cases and were associated with anaplastic histology, further supporting this conclusion. *MYOD1* is a skeletal muscle-specific transcription factor, which plays a key role in muscle development and differentiation. Kohsaka et al. reported that a recurrent somatic point mutation L122R in *MYOD1* is presented in a distinctive subset of ERMS with poor outcomes.[25] However, Rekhi et al. found that *MYOD1* L122R mutation occurred exclusively in SRMS, and were associated with a relatively aggressive clinical course.[38] Our data showed that *MYOD1* variant with L122R mutation occurred in 3 ERMS cases and 1 SRMS case, indicating a broader spectrum of tumor sub-types affected by this mutation and suggesting potential implications for clinical management and prognosis. ARID1A is the most frequently mutated subunit of SWI/SNF chromatin remodeling complexes across a variety of human cancers, and it functions as a tumor suppressor.[39] ARID1A loss impairs enhancer-mediated gene expression and drives cancers including neuroblastoma, colon cancer, and ovarian cancer.[23,24,40] ARID1B is synthetic lethal with ARID1A and knockdown of ARID1B in ARID1A-deficient backgrounds impairs cell proliferation in neuroblastoma and ovarian cancer cells.[23,24] Thus, mutations of *ARID1A* in RMS offer a potential therapeutic target for RMS.

In summary, we identified genetic mutations in 51 RMS specimens from the ZJUCH-RMS cohort and also established 9 PDCs from these samples. The RMS PDCs maintained the genetic mutations and the expression of RMS hallmark and dependency genes in matched primary tumors, serving as valuable tools for evaluating drug responses, and identifying gene-drug associations. With the increased number of validated RMS PDCs and the maturation of PDC-based platforms, we anticipate the provision of a robust and individualized preclinical model for the precise treatment of RMS. This advancement promises to enhance our understanding of RMS pathobiology and therapeutic responses, allowing for the identification of personalized treatment strategies tailored to the unique characteristics of each patient.

Limitations of the study

With the relatively lower success rate in establishing ARMS PDCs compared to ERMS, coupled with the limited availability of ARMS clinical samples, there is a need to expand the number of ARMS PDCs. Enhancements in methodologies are essential to improve the success rate for the establishment of ARMS PDCs, ultimately advancing our understanding of this aggressive subtype of RMS.
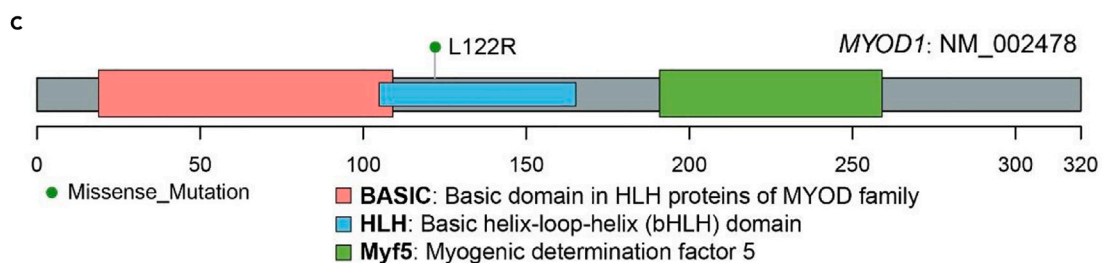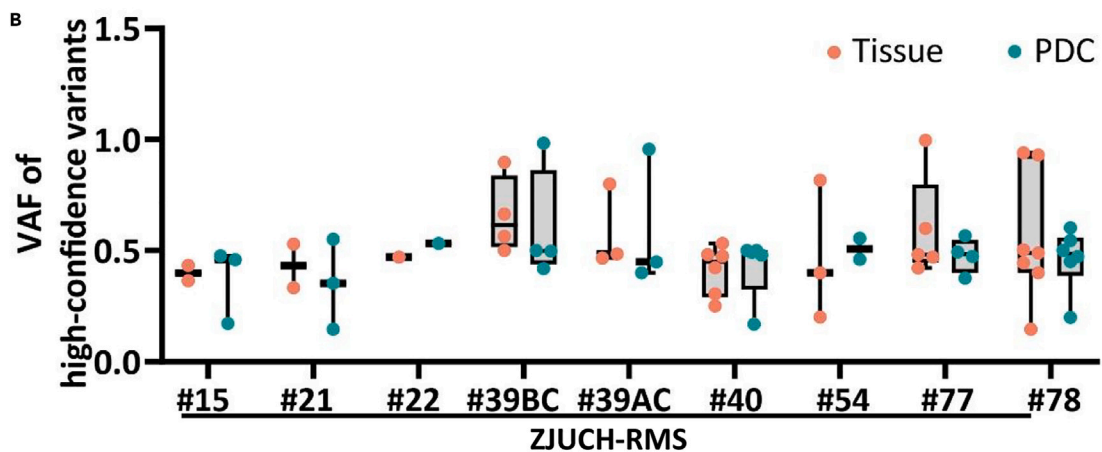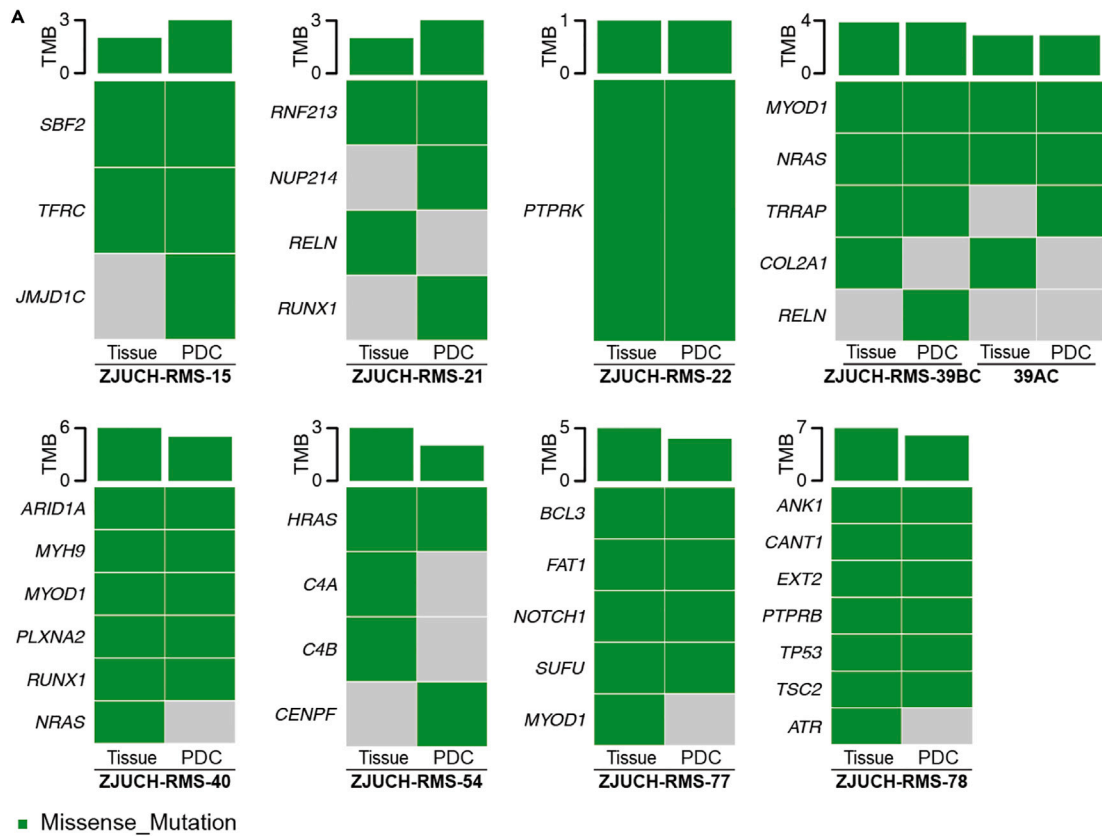
A

(Panels showing mutation matrices for TMB across samples ZJUCH-RMS-15, ZJUCH-RMS-21, ZJUCH-RMS-22, ZJUCH-RMS-39BC/39AC, ZJUCH-RMS-40, ZJUCH-RMS-54, ZJUCH-RMS-77, ZJUCH-RMS-78)

- ■ Missense_Mutation

B

(Box plot: VAF of high-confidence variants across ZJUCH-RMS samples #15, #21, #22, #39BC, #39AC, #40, #54, #77, #78; Tissue and PDC)

C

MYOD1: NM_002478

L122R

- ● Missense_Mutation
- ■ **BASIC**: Basic domain in HLH proteins of MYOD family
- ■ **HLH**: Basic helix-loop-helix (bHLH) domain
- ■ **Myf5**: Myogenic determination factor 5

Figure 5. RMS PDCs recapitulate the genetic alterations in matched primary tumors

(A) Oncoplots comparing genes with high-confidence mutations between RMS PDCs and matched primary tumors. TMB, tumor mutation burden.

(B) Variant allele frequency (VAF) of high-confidence variants identified from RMS PDCs and matched primary tumors. Boxes indicate the median (horizontal line), 25th percentile and 75th percentile; Whiskers, minimum or maximum value. Each dot represents the value for a single variant.

(C) A lollipop plot showing *MYOD1* variant with L122R mutation in the basic-helix-loop-helix (bHLH) domain. The protein domains of MYOD1 are shown.

RESOURCE AVAILABILITY

Lead contact

Further information and requests for resources and reagents should be directed to and will be fulfilled by the lead contact, Dr. Ting Tao (taot@zju.edu.cn).

Materials availability

All unique/stable reagents generated in this study are available from the lead contact with a completed Materials Transfer Agreement.

Data and code availability

- All related raw data in this study are available from the Genome Sequence Archive[41] in National Genomics Data Center,[42] China National Center for Bioinformation/Beijing Institute of Genomics, Chinese Academy of Sciences under accession number HRA007320 and HRA007324. All data present in this study will be shared by the lead contact upon request.
- This paper does not report original code.
- Any additional information required to reanalyze the data reported in this paper is available from the lead contact upon request.

AUTHOR CONTRIBUTIONS

T.T. and J.W. designed the study and experiments; Y.H., Z.H., S.L., M.H., X.W., and Y.T. collected the RMS samples; Y.H., Z.H., and S.L. performed the experiments; W.Y., Y.C., and M.Y. performed drug screening; T.T. and Z.H. performed the bioinformatics analysis; M.Z. and W.G. performed the pathology analysis; T.T., Z.H., and Y.H. drafted and finalized the manuscript with inputs from all other authors.

DECLARATION OF INTERESTS

The authors declare no competing interests.

STAR★METHODS

Detailed methods are provided in the online version of this paper and include the following:

- KEY RESOURCES TABLE
- EXPERIMENTAL MODEL AND STUDY PARTICIPANT DETAILS
  ○ Patient samples and characteristics
  ○ Patient-derived cell (PDC)
  ○ RMS cell lines
- METHOD DETAILS
  ○ RNA extraction and reverse transcription polymerase chain reaction (RT-PCR)
  ○ RNA sequencing (RNA-seq) and data analysis
  ○ Gene set enrichment analysis (GSEA)
  ○ Fluorescence *in situ* hybridization (FISH)
  ○ Immunofluorescence of RMS PDCs
  ○ Cell growth assay
  ○ The half-maximal inhibitory concentration (IC_{50}) assay
- QUANTIFICATION AND STATISTICAL ANALYSIS

SUPPLEMENTAL INFORMATION

Supplemental information can be found online at https://doi.org/10.1016/j.isci.2024.110862.
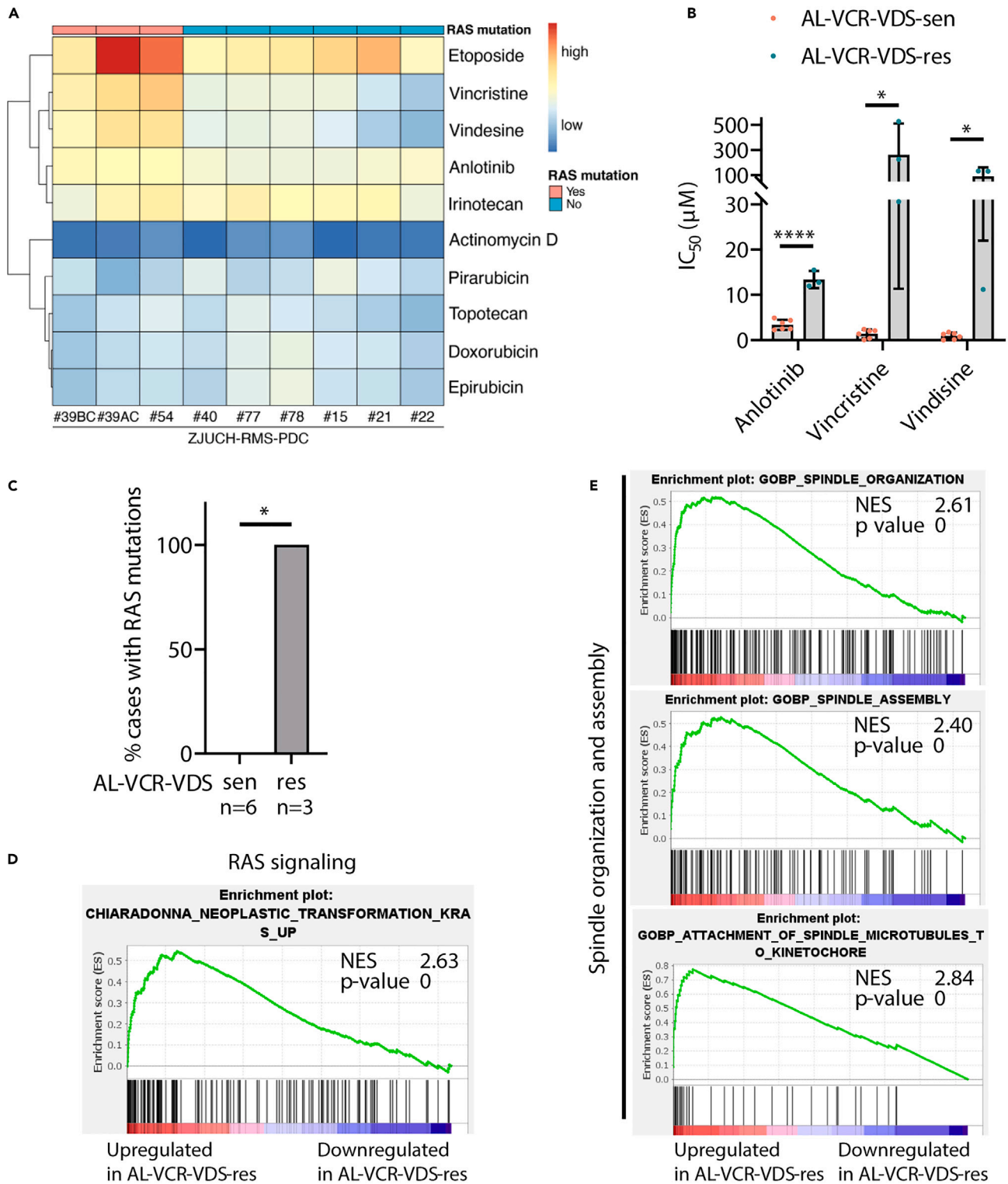
Figure 6. The effect of chemotherapeutic agents on RMS PDCs

(A) A clustered heatmap showing drug response profile based on $\log_{10}$ (IC_{50}) of common chemotherapeutic agents for nine RMS PDCs. Mutation status of *RAS* family genes was indicated.

(B) IC_{50} (μM) of anlotinib, vincristine, and vindesine for RMS PDCs in AL-VCR-VDS-sen and AL-VCR-VDS-res groups. Values are means $\pm$ SD. Each dot represents the value for a single RMS PDC. Mean values were compared by the two-tailed unpaired t test. *$p < 0.05$; ****$p < 0.0001$.

Figure 6. Continued

(C) Frequencies of mutations in *RAS* family genes (*NRAS*, *HRAS*, and *KRAS*) in AL-VCR-VDS-sen and AL-VCR-VDS-res groups were compared using the two-tailed Fisher's exact test. *$p < 0.05$.

(D and E) GSEA of gene expression profiles of RMS PDCs in AL-VCR-VDS-sen group versus AL-VCR-VDS-res group. Representative significantly enriched gene signatures indicative of RAS signaling (D) and spindle organization and assembly (E) are shown. Genes are ranked by score and plotted along the x axis as vertical black bars. NES, normalized enrichment score.

REFERENCES

1. Skapek, S.X., Ferrari, A., Gupta, A.A., Lupo, P.J., Butler, E., Shipley, J., Barr, F.G., and Hawkins, D.S. (2019). Rhabdomyosarcoma. Nat. Rev. Dis. Prim. *5*, 1. https://doi.org/10.1038/s41572-018-0051-2.

2. Martin-Giacalone, B.A., Weinstein, P.A., Plon, S.E., and Lupo, P.J. (2021). Pediatric Rhabdomyosarcoma: Epidemiology and Genetic Susceptibility. J. Clin. Med. *10*, 2028. https://doi.org/10.3390/jcm10092028.

3. Leiner, J., and Le Loarer, F. (2020). The current landscape of rhabdomyosarcomas: an update. Virchows Arch. *476*, 97–108. https://doi.org/10.1007/s00428-019-02676-9.

4. Gasparini, P., Casanova, M., Centonze, G., Borzi, C., Bergamaschi, L., Collini, P., Testi, A., Chiaravalli, S., Massimino, M., Sozzi, G., et al. (2023). Establishment of 6 pediatric rhabdomyosarcoma patient's derived xenograft models closely recapitulating patients' tumor characteristics. Tumori *109*, 314–323. https://doi.org/10.1177/03008916221110266.

5. WHO Classification of Tumours Editorial Board (2020). Soft tissue and bone tumours. WHO Classification of Tumours, *Volume 3*, 5th Edition.

6. Rudzinski, E.R., Kelsey, A., Vokuhl, C., Linardic, C.M., Shipley, J., Hettmer, S., Koscielniak, E., Hawkins, D.S., and Bisogno, G. (2021). Pathology of childhood rhabdomyosarcoma: A consensus opinion document from the Children's Oncology Group, European Paediatric Soft Tissue Sarcoma Study Group, and the Cooperative Weichteilsarkom Studiengruppe. Pediatr. Blood Cancer *68*, e28798. https://doi.org/10.1002/pbc.28798.

7. Haduong, J.H., Heske, C.M., Allen-Rhoades, W., Xue, W., Teot, L.A., Rodeberg, D.A., Donaldson, S.S., Weiss, A., Hawkins, D.S., and Venkatramani, R. (2022). An update on rhabdomyosarcoma risk stratification and the rationale for current and future Children's Oncology Group clinical trials. Pediatr. Blood Cancer *69*, e29511. https://doi.org/10.1002/pbc.29511.

8. Barretina, J., Caponigro, G., Stransky, N., Venkatesan, K., Margolin, A.A., Kim, S., Wilson, C.J., Lehár, J., Kryukov, G.V., Sonkin, D., et al. (2012). The Cancer Cell Line Encyclopedia enables predictive modelling of anticancer drug sensitivity. Nature *483*, 603–607. https://doi.org/10.1038/nature11003.

9. Garnett, M.J., Edelman, E.J., Heidorn, S.J., Greenman, C.D., Dastur, A., Lau, K.W., Greninger, P., Thompson, I.R., Luo, X., Soares, J., et al. (2012). Systematic identification of genomic markers of drug sensitivity in cancer cells. Nature *483*, 570–575. https://doi.org/10.1038/nature11005.

10. Hinson, A.R.P., Jones, R., Crose, L.E.S., Belyea, B.C., Barr, F.G., and Linardic, C.M. (2013). Human rhabdomyosarcoma cell lines for rhabdomyosarcoma research: utility and pitfalls. Front. Oncol. *3*, 183. https://doi.org/10.3389/fonc.2013.00183.

11. Lee, J.K., Liu, Z., Sa, J.K., Shin, S., Wang, J., Bordyuh, M., Cho, H.J., Elliott, O., Chu, T., Choi, S.W., et al. (2018). Pharmacogenomic landscape of patient-derived tumor cells informs precision oncology therapy. Nat. Genet. *50*, 1399–1411. https://doi.org/10.1038/s41588-018-0209-6.

12. Qiu, Z., Li, H., Zhang, Z., Zhu, Z., He, S., Wang, X., Wang, P., Qin, J., Zhuang, L., Wang, W., et al. (2019). A Pharmacogenomic Landscape in Human Liver Cancers. Cancer Cell *36*, 179–193.e11. https://doi.org/10.1016/j.ccell.2019.07.001.

13. Qiu, Z., Zou, K., Zhuang, L., Qin, J., Li, H., Li, C., Zhang, Z., Chen, X., Cen, J., Meng, Z., et al. (2016). Hepatocellular carcinoma cell lines retain the genomic and transcriptomic landscapes of primary human cancers. Sci. Rep. *6*, 27411. https://doi.org/10.1038/srep27411.

14. Patel, A.G., Chen, X., Huang, X., Clay, M.R., Komorova, N., Krasin, M.J., Pappo, A., Tillman, H., Orr, B.A., McEvoy, J., et al. (2022). The myogenesis program drives clonal selection and drug resistance in rhabdomyosarcoma. Dev. Cell *57*, 1226–1240.e8. https://doi.org/10.1016/j.devcel.2022.04.003.

15. Wei, Y., Qin, Q., Yan, C., Hayes, M.N., Garcia, S.P., Xi, H., Do, D., Jin, A.H., Eng, T.C., McCarthy, K.M., et al. (2022). Single-cell analysis and functional characterization uncover the stem cell hierarchies and developmental origins of rhabdomyosarcoma. Nat. Cancer *3*, 961–975. https://doi.org/10.1038/s43018-022-00414-w.

16. Danielli, S.G., Porpiglia, E., De Micheli, A.J., Navarro, N., Zellinger, M.J., Bechtold, I., Kisele, S., Volken, L., Marques, J.G., Kasper, S., et al. (2023). Single-cell profiling of alveolar rhabdomyosarcoma reveals RAS pathway inhibitors as cell-fate hijackers with therapeutic relevance. Sci. Adv. *9*, eade9238. https://doi.org/10.1126/sciadv.ade9238.

17. Gryder, B.E., Pomella, S., Sayers, C., Wu, X.S., Song, Y., Chiarella, A.M., Bagchi, S., Chou, H.C., Sinniah, R.S., Walton, A., et al. (2019). Histone hyperacetylation disrupts core gene regulatory architecture in rhabdomyosarcoma. Nat. Genet. *51*, 1714–1722. https://doi.org/10.1038/s41588-019-0534-4.

18. Gryder, B.E., Yohe, M.E., Chou, H.C., Zhang, X., Marques, J., Wachtel, M., Schaefer, B., Sen, N., Song, Y., Gualtieri, A., et al. (2017). PAX3-FOXO1 Establishes Myogenic Super Enhancers and Confers BET Bromodomain Vulnerability. Cancer Discov. *7*, 884–899. https://doi.org/10.1158/2159-8290.CD-16-1297.

19. Hettmer, S., and Wagers, A.J. (2010). Muscling in: Uncovering the origins of rhabdomyosarcoma. Nat. Med. *16*, 171–173. https://doi.org/10.1038/nm0210-171.

20. Tsherniak, A., Vazquez, F., Montgomery, P.G., Weir, B.A., Kryukov, G., Cowley, G.S., Gill, S., Harrington, W.F., Pantel, S., Krill-Burger, J.M., et al. (2017). Defining a Cancer Dependency Map. Cell *170*, 564–576.e16. https://doi.org/10.1016/j.cell.2017.06.010.

21. Pugh, T.J., Morozova, O., Attiyeh, E.F., Asgharzadeh, S., Wei, J.S., Auclair, D., Carter, S.L., Cibulskis, K., Hanna, M., Kiezun, A., et al. (2013). The genetic landscape of high-risk neuroblastoma. Nat. Genet. *45*, 279–284. https://doi.org/10.1038/ng.2529.

22. Wegert, J., Ishaque, N., Vardapour, R., Geörg, C., Gu, Z., Bieg, M., Ziegler, B., Bausenwein, S., Nourkami, N., Ludwig, N., et al. (2015). Mutations in the SIX1/2 pathway and the DROSHA/DGCR8 miRNA microprocessor complex underlie high-risk blastemal type Wilms tumors. Cancer Cell *27*, 298–311. https://doi.org/10.1016/j.ccell.2015.01.002.

23. Helming, K.C., Wang, X., Wilson, B.G., Vazquez, F., Haswell, J.R., Manchester, H.E., Kim, Y., Kryukov, G.V., Ghandi, M., Aguirre, A.J., et al. (2014). ARID1B is a specific vulnerability in ARID1A-mutant cancers. Nat. Med. *20*, 251–254. https://doi.org/10.1038/nm.3480.

24. Shi, H., Tao, T., Abraham, B.J., Durbin, A.D., Zimmerman, M.W., Kadoch, C., and Look, A.T. (2020). ARID1A loss in neuroblastoma promotes the adrenergic-to-mesenchymal transition by regulating enhancer-mediated gene expression. Sci. Adv. *6*, eaaz3440. https://doi.org/10.1126/sciadv.aaz3440.

25. Kohsaka, S., Shukla, N., Ameur, N., Ito, T., Ng, C.K.Y., Wang, L., Lim, D., Marchetti, A., Viale, A., Pirun, M., et al. (2014). A recurrent neomorphic mutation in MYOD1 defines a clinically aggressive subset of embryonal rhabdomyosarcoma associated with PI3K-AKT pathway mutations. Nat. Genet. *46*, 595–600. https://doi.org/10.1038/ng.2969.

26. Van Antwerp, M.E., Chen, D.G., Chang, C., and Prochownik, E.V. (1992). A point mutation in the MyoD basic domain imparts c-Myc-like properties. Proc. Natl. Acad. Sci. USA *89*, 9010–9014. https://doi.org/10.1073/pnas.89.19.9010.

27. Meng, Q., Han, J., Wang, P., Jia, C., Guan, M., Zhang, B., and Zhao, W. (2024). BMS-794833 reduces anlotinib resistance in osteosarcoma by targeting the VEGFR/Ras/CDK2 pathway. J. Bone Oncol. *45*, 100594. https://doi.org/10.1016/j.jbo.2024.100594.

28. Jerchel, I.S., Hoogkamer, A.Q., Ariës, I.M., Steeghs, E.M.P., Boer, J.M., Besselink, N.J.M., Boeree, A., van de Ven, C., de Groot-Kruseman, H.A., de Haas, V., et al. (2018). RAS pathway mutations as a predictive biomarker for treatment adaptation in pediatric B-cell precursor acute lymphoblastic leukemia. Leukemia *32*, 931–940. https://doi.org/10.1038/leu.2017.303.

29. Pudewell, S., Wittich, C., Kazemein Jasemi, N.S., Bazgir, F., and Ahmadian, M.R. (2021). Accessory proteins of the RAS-MAPK pathway: moving from the side line to the

front line. Commun. Biol. *4*, 696. https://doi.org/10.1038/s42003-021-02149-3.

30. Marques Da Costa, M.E., Zaidi, S., Scoazec, J.Y., Droit, R., Lim, W.C., Marchais, A., Salmon, J., Cherkaoui, S., Morscher, R.J., Laurent, A., et al. (2023). A biobank of pediatric patient-derived-xenograft models in cancer precision medicine trial MAPPYACTS for relapsed and refractory tumors. Commun. Biol. *6*, 949. https://doi.org/10.1038/s42003-023-05320-0.

31. Meister, M.T., Groot Koerkamp, M.J.A., de Souza, T., Breunis, W.B., Frazer-Mendelewska, E., Brok, M., DeMartino, J., Manders, F., Calandrini, C., Kerstens, H.H.D., et al. (2022). Mesenchymal tumor organoid models recapitulate rhabdomyosarcoma subtypes. EMBO Mol. Med. *14*, e16001. https://doi.org/10.15252/emmm.202216001.

32. Stewart, E., Federico, S.M., Chen, X., Shelat, A.A., Bradley, C., Gordon, B., Karlstrom, A., Twarog, N.R., Clay, M.R., Bahrami, A., et al. (2017). Orthotopic patient-derived xenografts of paediatric solid tumours. Nature *549*, 96–100. https://doi.org/10.1038/nature23647.

33. Manzella, G., Schreck, L.D., Breunis, W.B., Molenaar, J., Merks, H., Barr, F.G., Sun, W., Römmele, M., Zhang, L., Tchinda, J., et al. (2020). Phenotypic profiling with a living biobank of primary rhabdomyosarcoma unravels disease heterogeneity and AKT sensitivity. Nat. Commun. *11*, 4629. https://doi.org/10.1038/s41467-020-18388-7.

34. Shern, J.F., Chen, L., Chmielecki, J., Wei, J.S., Patidar, R., Rosenberg, M., Ambrogio, L., Auclair, D., Wang, J., Song, Y.K., et al. (2014). Comprehensive genomic analysis of rhabdomyosarcoma reveals a landscape of alterations affecting a common genetic axis in fusion-positive and fusion-negative tumors. Cancer Discov. *4*, 216–231. https://doi.org/10.1158/2159-8290.CD-13-0639.

35. Shern, J.F., Selfe, J., Izquierdo, E., Patidar, R., Chou, H.C., Song, Y.K., Yohe, M.E., Sindiri, S., Wei, J., Wen, X., et al. (2021). Genomic Classification and Clinical Outcome in Rhabdomyosarcoma: A Report From an International Consortium. J. Clin. Oncol. *39*, 2859–2871. https://doi.org/10.1200/JCO.20.03060.

36. Ramadan, F., Fahs, A., Ghayad, S.E., and Saab, R. (2020). Signaling pathways in Rhabdomyosarcoma invasion and metastasis. Cancer Metastasis Rev. *39*, 287–301. https://doi.org/10.1007/s10555-020-09860-3.

37. Hettmer, S., Archer, N.M., Somers, G.R., Novokmet, A., Wagers, A.J., Diller, L., Rodriguez-Galindo, C., Teot, L.A., and Malkin, D. (2014). Anaplastic rhabdomyosarcoma in TP53 germline mutation carriers. Cancer *120*, 1068–1075. https://doi.org/10.1002/cncr.28507.

38. Rekhi, B., Upadhyay, P., Ramteke, M.P., and Dutt, A. (2016). MYOD1 (L122R) mutations are associated with spindle cell and sclerosing rhabdomyosarcomas with aggressive clinical outcomes. Mod. Pathol. *29*, 1532–1540. https://doi.org/10.1038/modpathol.2016.144.

39. Kadoch, C., Hargreaves, D.C., Hodges, C., Elias, L., Ho, L., Ranish, J., and Crabtree, G.R. (2013). Proteomic and bioinformatic analysis of mammalian SWI/SNF complexes identifies extensive roles in human malignancy. Nat. Genet. *45*, 592–601. https://doi.org/10.1038/ng.2628.

40. Mathur, R., Alver, B.H., San Roman, A.K., Wilson, B.G., Wang, X., Agoston, A.T., Park, P.J., Shivdasani, R.A., and Roberts, C.W.M. (2017). ARID1A loss impairs enhancer-mediated gene regulation and drives colon cancer in mice. Nat. Genet. *49*, 296–302. https://doi.org/10.1038/ng.3744.

41. Chen, T., Chen, X., Zhang, S., Zhu, J., Tang, B., Wang, A., Dong, L., Zhang, Z., Yu, C., Sun, Y., et al. (2021). The Genome Sequence Archive Family: Toward Explosive Data Growth and Diverse Data Types. Dev. Reprod. Biol. *19*, 578–583. https://doi.org/10.1016/j.gpb.2021.08.001.

42. CNCB-NGDC Members and Partners (2022). Database Resources of the National Genomics Data Center, China National Center for Bioinformation in 2022. Nucleic Acids Res. *50*, D27–D38. https://doi.org/10.1093/nar/gkab951.

43. Dobin, A., Davis, C.A., Schlesinger, F., Drenkow, J., Zaleski, C., Jha, S., Batut, P., Chaisson, M., and Gingeras, T.R. (2013). STAR: ultrafast universal RNA-seq aligner. Bioinformatics *29*, 15–21. https://doi.org/10.1093/bioinformatics/bts635.

44. Wang, K., Li, M., and Hakonarson, H. (2010). ANNOVAR: functional annotation of genetic variants from high-throughput sequencing data. Nucleic Acids Res. *38*, e164. https://doi.org/10.1093/nar/gkq603.

45. Edmonson, M.N., Patel, A.N., Hedges, D.J., Wang, Z., Rampersaud, E., Kesserwan, C.A., Zhou, X., Liu, Y., Newman, S., Rusch, M.C., et al. (2019). Pediatric Cancer Variant Pathogenicity Information Exchange (PeCanPIE): a cloud-based platform for curating and classifying germline variants. Genome Res. *29*, 1555–1565. https://doi.org/10.1101/gr.250357.119.

46. Anders, S., and Huber, W. (2010). Differential expression analysis for sequence count data. Genome Biol. *11*, R106. https://doi.org/10.1186/gb-2010-11-10-r106.

47. Mayakonda, A., Lin, D.C., Assenov, Y., Plass, C., and Koeffler, H.P. (2018). Maftools: efficient and comprehensive analysis of somatic variants in cancer. Genome Res. *28*, 1747–1756. https://doi.org/10.1101/gr.239244.118.

48. Subramanian, A., Tamayo, P., Mootha, V.K., Mukherjee, S., Ebert, B.L., Gillette, M.A., Paulovich, A., Pomeroy, S.L., Golub, T.R., Lander, E.S., and Mesirov, J.P. (2005). Gene set enrichment analysis: a knowledge-based approach for interpreting genome-wide expression profiles. Proc. Natl. Acad. Sci. USA *102*, 15545–15550. https://doi.org/10.1073/pnas.0506580102.

49. Liao, Y., Smyth, G.K., and Shi, W. (2014). featureCounts: an efficient general purpose program for assigning sequence reads to genomic features. Bioinformatics *30*, 923–930. https://doi.org/10.1093/bioinformatics/btt656.

50. Landrum, M.J., Chitipiralla, S., Brown, G.R., Chen, C., Gu, B., Hart, J., Hoffman, D., Jang, W., Kaur, K., Liu, C., et al. (2020). ClinVar: improvements to accessing data. Nucleic Acids Res. *48*, D835–D844. https://doi.org/10.1093/nar/gkz972.

51. Li, Q., and Wang, K. (2017). InterVar: Clinical Interpretation of Genetic Variants by the 2015 ACMG-AMP Guidelines. Am. J. Hum. Genet. *100*, 267–280. https://doi.org/10.1016/j.ajhg.2017.01.004.

52. Chakravarty, D., Gao, J., Phillips, S.M., Kundra, R., Zhang, H., Wang, J., Rudolph, J.E., Yaeger, R., Soumerai, T., Nissan, M.H., et al. (2017). OncoKB: A Precision Oncology Knowledge Base. JCO Precis. Oncol. *1*, 1–16. https://doi.org/10.1200/PO.17.00011.

53. Tate, J.G., Bamford, S., Jubb, H.C., Sondka, Z., Beare, D.M., Bindal, N., Boutselakis, H., Cole, C.G., Creatore, C., Dawson, E., et al. (2019). COSMIC: the Catalogue Of Somatic Mutations In Cancer. Nucleic Acids Res. *47*, D941–D947. https://doi.org/10.1093/nar/gky1015.

54. Maeser, D., Gruener, R.F., and Huang, R.S. (2021). oncoPredict: an R package for predicting *in vivo* or cancer patient drug response and biomarkers from cell line screening data. Brief Bioinform *22*, bbab260. https://doi.org/10.1093/bib/bbab260.

STAR★METHODS

KEY RESOURCES TABLE

REAGENT or RESOURCE	SOURCE	IDENTIFIER
Antibodies		
Anti-MYOD1 antibody	Cell Signaling Technology	Cat# 13812; RRID: AB_2798320
Anti-MYOD1 antibody	GeneTech	Cat# GT218802
Anti-MYOG antibody	Abcam	Cat# ab219998
Anti-MYOG antibody	GeneTech	Cat# GM355929
Goat anti-Rabbit IgG (H+L) Highly Cross-Adsorbed Secondary Antibody, Alexa Fluor™ 488	Thermo Fisher Scientific	Cat# A-11034; RRID: AB_2576217
Biological samples		
Human Rhabdomyosarcoma	This paper	N/A
Chemicals, peptides, and recombinant proteins		
Compound for screening, see Table S6	Selleck, MCE	see Table S6
Critical commercial assays		
HiScript III All-in-one RT SuperMix Perfect for qPCR	Vazyme	Cat# R333
MycoBlue Mycoplasma Detector	Vazyme	Cat# D101
CellTiter-Glo Luminescent Cell Viability Assay	Promega	Cat# G7573
Cell Counting Kit-8	TargetMol	Cat# C0005
Deposited data		
RNA-seq data	This paper	CNCB: HRA007320, HRA007324
Experimental models: Cell lines		
PLA-802	Laboratory stock	N/A
RH30	American Type Culture Collection	Cat# CRL-2061
RD	National Collection of Authenticated Cell Cultures	Cat# TCHu 45
Other		
ZJUCH-RMS-PDC-15	This paper	N/A
ZJUCH-RMS-PDC-21	This paper	N/A
ZJUCH-RMS-PDC-22	This paper	N/A
ZJUCH-RMS-PDC-39BC	This paper	N/A
ZJUCH-RMS-PDC-39AC	This paper	N/A
ZJUCH-RMS-PDC-40	This paper	N/A
ZJUCH-RMS-PDC-54	This paper	N/A
ZJUCH-RMS-PDC-77	This paper	N/A
ZJUCH-RMS-PDC-78	This paper	N/A
Oligonucleotides		
Primers for RT-PCR, see Table S8	This paper	N/A
Software and algorithms		
GraphPad Prism 9	GraphPad software	www.graphpad.com
STAR	Dobin et al., 2013[43]	https://github.com/alexdobin/STAR
CTAT-Mutations	Github	https://github.com/NCIP/ctat-mutations

Continued		
REAGENT or RESOURCE	SOURCE	IDENTIFIER
ANNOVAR	Wang et al., 2010[44]	https://annovar.openbioinformatics.org/en/latest
PeCanPIE	Edmonson et al., 2019[45]	https://pecan.stjude.cloud/pie
DESeq2 package	Anders and Huber, 2010[46]	https://bioconductor.org/packages//2.12/bioc/html/DESeq2.html
maftools	Mayakonda et al., 2018[47]	https://bioconductor.riken.jp/packages/3.4/bioc/html/maftools.html
Gene Set Enrichment Analysis (GSEA)	Subramanian et al., 2005[48]	https://www.gsea-msigdb.org/gsea/index.jsp

EXPERIMENTAL MODEL AND STUDY PARTICIPANT DETAILS

Patient samples and characteristics

Rhabdomyosarcoma samples were obtained from Department of Surgical Oncology, Children's Hospital Zhejiang University School of Medicine, and these samples were referred to as ZJUCH-RMS cohort. The demographic characteristics of patient samples are presented as Tables S1 and S2. This study was approved by the Ethics Committee of Children's Hospital, Zhejiang University School of Medicine (2020-IRB-049). All data were acquired with informed consent from patients, their parents or guardians. All results were reported with arbitrary sample ID numbers without linked identifiers. Histopathological features of these tumors were evaluated by department of pathology, Children's Hospital Zhejiang University School of Medicine. Briefly, the tissue specimen was fixed in 10% neutral buffered formalin, routinely processed, and embedded in paraffin. Paraffin blocks were used to generate haematoxylin and eosin (H&E)-stained sections. Immunohistochemistry for MYOD1 (clone EP212, diluted 1:200; GeneTech) and MYOG (clone EP162, diluted 1:200; GeneTech) was performed on 4-μm-thick tissue sections using the BenchMark ULTRA automated immunostainer (Ventana Medical Systems, Tucson, USA).

Patient-derived cell (PDC)

RMS tissues were obtained from post-surgical resection and rinsed with PBS. Both necrotic tissues and blood vessels were removed, and the remaining tissues were delicately dissected into small fragments or cubes (1 to 2 mm in diameter) with scissors and scalpels. The resuspended cancer fragments were washed with DMEM/F-12 (1:1) medium (VivaCell) in a 70 μm cell strainer, and transferred into a tissue culture dishes containing pre-warmed DMEM/F-12 (1:1) medium (VivaCell) supplemented with 15% fetal bovine serum (ExCell) and 1X penicillin-streptomycin-amphotericin B (Solarbio). The culture dishes were incubated in a CO_2 incubator set to 37°C with 5% CO_2, and the growth of the adherent cells was closely monitored. The absence of mycoplasma contamination was confirmed by MycoBlue Mycoplasma Detector (Vazyme #D101). RMS PDCs were validated by the expression of RMS hallmark genes including MYOD1, MYOG, MYF5 and DES.

RMS cell lines

RMS cell line RH30 was purchased from American Type Culture Collection (ATCC), RD from National Collection of Authenticated Cell Cultures (NCACC, Shanghai, China), and PLA-802 as a laboratory stock. They were maintained in DMEM medium (VivaCell) supplemented with 10% fetal bovine serum (ExCell) and 1X penicillin-streptomycin-amphotericin B (Solarbio). The absence of mycoplasma contamination was confirmed by MycoBlue Mycoplasma Detector (Vazyme #D101).

METHOD DETAILS

RNA extraction and reverse transcription polymerase chain reaction (RT-PCR)

Total RNA from RMS PDCs was extracted by the TRIzol reagent (Thermo Fisher Scientific #15596018CN). For RT-PCR, genomic DNA was removed and first-strand cDNA was synthesized using the HiScript III All-in-one RT SuperMix Perfect for qPCR (Vazyme #R333), and RT-PCR was performed on ProFlex PCR System (Thermo Fisher Scientific) according to the manufacturer's instructions. Primer pairs for amplification are listed in Table S8.

RNA sequencing (RNA-seq) and data analysis

Total RNA from RMS PDCs and primary tumors was extracted by the TRIzol reagent (Thermo Fisher Scientific #15596018CN), and subjected to library preparation for Illumina NovaSeq 6000 S4 sequencing with a 150 bp paired-end sequencing strategy at Zhejiang Biosan Biochemical Technologies Co., Ltd. RNA-seq data were aligned to the GRCh38 reference genome with STAR (2-passing mapping),[43] followed by duplicates marking with Picard (https://broadinstitute.github.io/picard/), and reads mapped to each gene were counted by featureCounts.[49] Differentially expressed genes were called by the R Bioconductor package DESeq2,[46] and normalized expression values for individual samples were obtained from DESeq2 using the variance-stabilizing transformation of the raw counts. The variance-stabilizing transformed data were used for gene set enrichment analysis (GSEA).

For mutational analysis, RNA-seq data were processed through CTAT-Mutations, a machine learning based RNA-seq variant calling pipeline (https://github.com/NCIP/ctat-mutations). Through CTAT-Mutations, RNA-seq data were processed with GATK best practices along with downstream annotation and filtration of variants. The results were further annotated with ANNOVAR,[44] and potential tumor-associated mutations were identified through the following steps. First, variants were excluded if they met any of the following criteria: 1) variants not located in exonic or splicing regions, or are synonymous SNVs located in exonic region, or located in repetitive regions of the genome; 2) variants with allele reads less than 3, or sequencing depth less than 8; 3) VAF < 0.1 or allele frequency greater than 0.01 in ExAC or 1000 Genomes database. The candidate variants were selected from the retained variants if they met any of the following criteria: 1) variants were annotated as "pathogenic, "likely pathogenic", "affects", "confers_sensitivity", "association", "drug response" or "risk factor" in ClinVar or InterVar databases,[50,51] or annotated as "oncogenic" or "likely oncogenic" in OncoKB,[52] or presented in the COSMIC cancer gene census v97 database[53]; 2) variants not predicted to be unharmful by all of the following programmes: SIFT, Polyphen2_HVAR, Polyphen2_HDIV, LRT, MutationTaster, MutationAssessor, FATHMM and ClinPred. The candidate variants were further annotated with PeCanPIE,[45] and only variants classified with a medal were considered as high-confidence mutations. Variants were visualized using R package maftools.[47] The GO analysis was performed using the PANTHER Overrepresentation Test (Released 20240226) (https://www.pantherdb.org/).

Gene set enrichment analysis (GSEA)

Genes from whole transcriptomic data were ranked based on the stat from DESeq2. The pre-ranked option of GSEA[48] was run with 1000 permutations for statistical evaluation. GSEA was performed with signatures from version 7.4 of the molecular signature database (MolSigDB) (http://www.broadinstitute.org/gsea/msigdb/index.jsp).

Fluorescence *in situ* hybridization (FISH)

The interruption of *PAX3* or *FOXO1* gene was assessed by FISH. Tissue sections at 4-μm-thick were prepared from formalin-fixed, paraffin-embedded (FFPE) tissue blocks. The sections, along with *PAX3* or *FOXO1* break-apart probes (Anbiping Medicine Science and Technology #F.01227-01, #F.01018-01), were co-denatured at 90°C for 5 minutes, then incubated at 37°C for 18 hours using the ThermoBrite Elite denaturation-hybridization system (Leica Biosystems). A minimum of 200 tumor cell nuclei were analyzed. Gene rearrangement was identified by a split signal, defined as the separation of signals by more than two signal widths. A positive result was defined as more than 20% of the assessed nuclei displaying split signals.

Immunofluorescence of RMS PDCs

For immunofluorescence staining of RMS PDCs, cells on coverslips were washed twice in PBS, fixed in 3% paraformaldehyde at 4°C for 30 minutes. After incubating 3 times with 50mM NH4Cl in PBS and permeabilizing with PBS/0.2% Triton X-100 at room temperature for 15 min, the cells were incubated with an anti-MYOD1 rabbit monoclonal (D8G3) antibody (Cell Signaling Technology #13812) or an anti-MYOG rabbit polyclonal antibody (Abcam #ab219998) for 2 hours, washed by PBS/0.2% Triton X-100, and then incubated with a secondary antibody conjugated with Alexa Flour 488 ((Thermo Fisher Scientific #A-11034) for 1 hour. DAPI (SouthernBiotech #0100-20) was used for nuclear staining.

Cell growth assay

RMS PDCs were seeded into a 96-well plate at a density of 2000 cells per well. Relative cell growth at days 1, 2, 3, 4 and 5 was evaluated by CellTiter-Glo Luminescent Cell Viability Assay (Promega #G7573).

The half-maximal inhibitory concentration (IC$_{50}$) assay

For the large-scale screening of the targeted anti-cancer drugs and chemotherapeutic agents, RMS PDCs were seeded into a 384-well plate at a density of 500 cells per well one day before treatment. For the test of common chemotherapeutic agents, RMS PDCs were seeded into a 96-well plate at a density of 5000 cells per well one day before treatment. After 3 days treatment with vehicle (DMSO) or compounds at various concentrations, relative cell growth was evaluated by CellTiter-Glo Luminescent Cell Viability Assay (Promega #G7571) or Cell Counting Kit-8 (CCK-8) (TargetMol #C0005) as a percentage of the vehicle (DMSO) control. The IC$_{50}$ value was determined with GraphPad Prism 9. The relationship between gene mutation and drug sensitivity was predicted by an R package oncoPredict.[54]

QUANTIFICATION AND STATISTICAL ANALYSIS

Statistical analyses were performed using two-tailed Fisher's exact test or two-tailed unpaired *t*-test, as indicated in each of the figure legend. $p < 0.05$ was considered as statistically significant.